HHS Public Access

Author manuscript

J Toxicol Environ Health A. Author manuscript; available in PMC 2016 January 05.

Published in final edited form as:

J Toxicol Environ Health A. 2014 ; 77(20): 1251–1268. doi:10.1080/15287394.2014.897490.

THE EFFECT OF TUNGSTATE NANOPARTICLES ON REACTIVE OXYGEN SPECIES AND CYTOTOXICITY IN RAW 264.7 MOUSE MONOCYTE MACROPHAGE CELLS

Katherine M. Dunnick[1,2], **Melissa A. Badding**[1], **Diane Schwegler-Berry**[1], **Jonathan M. Patete**[3], **Christopher Koenigsmann**[3], **Stanislaus S. Wong**[3,4], and **Stephen S. Leonard**[1,2]

[1]National Institute for Occupational Safety and Health, HELD, Morgantown, West Virginia, USA

[2]West Virginia University, Pharmaceutical and Pharmacological Sciences, Morgantown, West Virginia, USA

[3]Department of Chemistry, State University of New York at Stony Brook, Stony Brook, New York, USA

[4]Condensed Matter Physics and Materials Sciences Department, Brookhaven National Laboratory, Upton, New York, USA

Abstract

Due to their unique size, surface area, and chemical characteristics, nanoparticles' use in consumer products has increased. However, the toxicity of nanoparticle (NP) exposure during the manufacturing process has not been fully assessed. Tungstate NP are used in numerous products, including but not limited to scintillator detectors and fluorescent lighting. As with many NP, no apparent toxicity studies have been completed with tungstate NP. The hypothesis that tungstate NP in vitro exposure results in reactive oxygen species (ROS) formation and cytotoxicity was examined. Differences in toxicity based on tungstate NP size, shape (sphere vs. wire), and chemical characteristics were determined. RAW 264.7 mouse monocyte macrophages were exposed to tungstate NP, and ROS formation was assessed via electron spin resonance (ESR), and several assays including hydrogen peroxide, intracellular ROS, and Comet. Results showed ROS production induced by tungstate nanowire exposure, but this exposure did not result in oxidative DNA damage. Nanospheres showed neither ROS nor DNA damage following cellular exposure. Cells were exposed over 72 h to assess cytotoxicity using an MTT (tetrazolium compound) assay. Results showed that differences in cell death between wires and spheres occurred at 24 h but were minimal at both 48 and 72 h. The present results indicate that tungstate nanowires are more reactive and produce cell death within 24 h of exposure, whereas nanospheres are less reactive and did not produce cell death. Results suggest that differences in shape may affect reactivity.

Address correspondence to Katherine M. Dunnick, NIOSH, HELD, PPRB, 1095 Willowdale Rd, Morgantown, WV 26505, USA. kdunnick@mix.wvu.edu.

SUPPLEMENTAL DATA

Supplemental data for this article can be accessed at http://dx.doi.org/10.1080/15287394.2014.897490

DISCLAIMER

The findings and conclusions of this work have not been formally disseminated by NIOSH and should not be construed to represent any agency determination or policy.

However, regardless of the differences in reactivity, in general both shapes produced mild ROS and resulted in minimal cell death at 48 and 72 h in RAW 264.7 cells.

Nanoparticles (NP) are defined as any structure with one dimension between 1 and 100 nm (Love et al., 2012). Their small size and large surface area-to-volume ratios offer physical and chemical properties not necessarily found in larger particles of similar chemical composition. For these reasons, increases in their manufacturing as well as in their commercial application and use have been rising dramatically (Zhao and Castranova, 2011). Such increases may result in novel occupational exposures and potential health hazards that are dependent on the toxicity of the NP. It is therefore important to understand potential risks associated with NP use. Nanoscale zinc oxide (ZnO) is currently being used in sunscreens to remove the unpleasant white film commonly associated with sunscreen application (Monteiro-Riviere et al., 2011). Unfortunately, studies showed that while nanosized ZnO is useful in sunscreen coloring, the reduced size also may result in increased toxicity (Chung et al., 2013; Xia et al., 2008). Due to the potential for toxic worker exposures, it is important to assess whether the benefits of nanomaterials are indeed worth the health risks.

Nanoscale metal oxides represent one such material for which an increase in their usage has been noted. Currently they are incorporated as components of gas sensors, as they increase performance and reduce instabilities observed with their polycrystalline counterparts (Comini, 2006). However, their unique properties have been speculated to be partly responsible for their biological toxicology (Nel et al., 2006). Metal oxides, for example, are widely known for their semiconducting properties, allowing for passive electron transfer between the nanomaterial and aqueous environments. This passive electron transfer is thought to play a role in toxicity, as it may occur between the metal oxides and the biological or cellular system, thereby promoting oxidative stress and inflammation (Roberts et al., 2011; Zhang et al., 2012). Studies demonstrated that metal oxide NP are capable of inducing reactive oxygen species (ROS) formation, which results in oxidative stress, DNA damage, and downstream health effects such as inflammatory responses (Karlsson et al., 2009; Moon et al., 2010; Rushton et al., 2010; Xia et al., 2008; Zhang et al., 2012). Studies also showed that metal oxides, specifically ZnO, induce lactose dehydrogenase (LDH) leakage and apoptosis at low (50 μg/ml) NP doses and necrosis at high (100 μg/ml) NP doses (Jeng and Swanson, 2006). Therefore, a dose of 50 μg/ml was chosen for this toxicity study as an intermediate concentration that was predicted to elicit a cellular response.

The growing use of nanomaterials in consumer products has resulted in increased industrial manufacturing (Zhao and Castranova, 2011). Tungstate NP, whose possible applications include fluorescent lighting, scintillator detectors, and gas sensors (Zhang et al., 2008a, 2008b), represent one such metal oxide that may be associated with increased manufacturing activity in the future. However, to date, no apparent studies have been performed on tungstate NP toxicity. Therefore, our study focused on assessing the acute toxicity of six different alkaline earth metal tungstate nanowires and six different nanospheres AWO_4 (A = Ca, Sr, Ba) in an in vitro model. Further, data demonstrated that NP of similar or identical chemical composition vary in toxicity based on size or shape (Yang et al., 2009). Thus, the

aim of this study was to examine how differences in size, shape, and chemical composition correlate with toxicity. Based on previous studies that found metal oxide toxicity in RAW 264.7 cells (Heng et al., 2011; Kang et al., 2008), it was postulated that tungstate NP exposure might generate ROS and promote cell death. Further, it was postulated that differences in size and shape of the NP may affect toxicity.

MATERIALS AND METHODS

Cell Culture

RAW 264.7 mouse monocyte macrophage cells (ATCC, Rockville, MD) were cultured following the ATCC recommended protocol. Cells were cultured in Dulbecco's modified Eagle's medium (DMEM) with 2 m*M* L-glutamine, 10% fetal bovine serum (FBS), and 50 mg/ml penicillin/streptomycin (Thermo Scientific, Pittsburgh, PA). Cells were grown at 37°C in a 5% CO_2 incubator and passaged by scraping into medium. RAW 264.7 cells were selected for these studies because they react with and engulf particles.

Tungstate Nanoparticle (NP) Production and Characterization

A commercially available, track-etched polycarbonate membrane, possessing pores with an average diameter of 50 nm, was mounted between two halves of a U-shaped reaction tube. Each half contained aqueous precursor solutions of defined chemical composition, which were allowed to diffuse toward each other, so as to control the resulting spatially confined growth of the corresponding anisotropic NP within the hollow membrane pore channels. In a typical synthesis of tungstate nanowires, one of the two half cells was filled with Na_2WO_4 solution, and the other half cell contained a solution of the metal salt (either $CaCl_2$, $SrCl_2$, or $Ba(NO_3)_2$), to correspondingly generate $CaWO_4$, $SrWO_4$, and $BaWO_4$ nanowires (Zhang et al., 2008a). For the aggregates of tungstate nanospheres, the synthesis was accomplished by solution-phase precipitation of the appropriate alkali earth metal salt (either $CaCl_2$, $SrCl_2$, or $Ba(NO_3)_2$) and sodium tungstate Na_2WO_4 (Thongtem et al., 2010).

Purity was assessed using x-ray diffraction (XRD) and dimensions (diameter and length) of NP were determined using a field emission scanning electron microscopy (SEM) instrument (Zhang et al., 2008a). To prepare XRD samples, the tungstate NP were rendered into slurries in ethanol, sonicated, and subsequently air-dried as a film upon deposition onto glass slides. Multiple, replicate diffraction patterns were collected using a Scintag diffractometer (Scintag, Inc., Cupertino, CA), operating in the Bragg–Brentano configuration using Cu Kα radiation (λ = 1.54 Å) from 10° to 80° at a scanning rate of 2°/min.

The dimensions as well as morphology of as-prepared tungstate NP were characterized using a field emission scanning electron microscopy instrument (FE-SEM Leo 1550), operating at an accelerating voltage of 15 kV and equipped with energy-dispersive x-ray spectroscopy (EDS) capabilities. Samples for SEM were prepared by dispersing as-prepared tungstate NP in ethanol, sonicating for about 2 min, and then depositing a dilute solution of the sample onto either a conductive tape or a silicon wafer, attached to a SEM brass stub. All of these samples were then conductively coated with gold by sputtering for 15 s so as to minimize charging effects under SEM imaging conditions.

Agglomeration and size distribution of tungstate NP in a suspended state were assessed using dynamic light scattering (DLS). DLS analyzes the velocity distribution of suspended particles by detecting fluctuations of light scattering intensity produced by Brownian motion of the particles. This technique yields a hydrodynamic radius or diameter of the particles. Tungstate NP were prepared in dispersion media at concentrations of 100 μg/ml and a Nanotrac 252 (Microtrac, Montgomeryville, PA) was used to assess diameter and agglomeration.

Determination of Cellular Interaction With Tungstate Nanoparticles

RAW 264.7 cells were grown on cleaned, autoclaved coverglass until 60–80% confluent (Chemglass Life Sciences, Vineland, NJ). Tungstate NP were prepared in dispersion media at a stock concentration of 1 mg/ml, as previously described (Porter et al., 2008). Cells were then exposed to tungstate NP at a final concentration of 10 μg/ml for 5 min, 1 h, 3 h, or 7 h in serum-free media. Following incubation, the media were removed and cells were washed 3 times with warm phosphate-buffered saline (PBS), fixed with 10% formalin for 10 min, washed 3 times with PBS, mounted with Fluoromount G, and sealed with clear nail polish. Slides used for this experiment were purchased as clean cut slides (Schott Nexterion, Arlington, VA) to prevent excess silica particle residue, which results in excessive background during imaging. Following mounting, images were acquired at 60× magnification using a Cytoviva enhanced dark-field microscopy system (Aetos Technologies, Inc., Auburn, AL) integrated into an Olympus BX41 upright optical microscope equipped with an Olympus DP73 digital camera (Olympus, Center Valley, PA). An enhanced dark-field microscope allows visualization of nanosized particles that would otherwise not be visible under typical light microscopy (Gibbs-Flournoy et al., 2011). Cellular interaction was determined as the number of cells associated with particles relative to the number of cells not associated with particles. At a minimum, 50 cells were counted; any cell that had a bright spot associated was considered a positive, while any cell lacking bright spots was considered a negative or unassociated cell. The relative association is expressed as a percentage.

For SEM, RAW 264.7 cells were grown on cleaned, autoclaved coverglass until 60–80% confluent (Chemglass Life Sciences, Vineland, NJ). Tungstate NP were prepared in dispersion media at a stock concentration of 1 mg/ml. Cells were exposed at a final concentration of 10 μg/ml tungstate NP in serum-free media for 3 h. Following exposure, cells were washed three times with warm PBS to remove unbound particles. The samples were fixed in formalin and postfixed in osmium tetroxide, dehydrated in an ethanol series, dried using hexamethyldisalizane, mounted onto aluminum stubs, and sputter-coated with gold/palladium to render them conductive. The samples were then imaged on a Hitachi S-4800 field emission scanning electron microscope (Hitachi High Technologies America, Inc., Clarksburg, MD). Elemental analysis was performed on samples to ensure particles associated with cells were tungstate NP using an energy-dispersive system attachment. The electron beam was pointed at the area of the sample to be analyzed, resulting in an x-ray spectrum characteristic of the elemental composition of the sample. Only elements present within the area were emitted and recorded on the spectral graph.

Determination of Cellular Engulfment of Tungstate Nanoparticles

For transmission electron microscopy (TEM), RAW 264.7 cells were grown in six-well dishes until confluent. Cells were exposed to tungstate NP at 50 μg/ml for 3 h in serum-free media. Following exposure, media were removed and cells scraped into 1 ml PBS, and centrifuged at 500 × g for 5 min. The samples were then fixed in Karnovsky's (2.5% gluteraldehyde, 2.5% paraformaldehyde in 0.1 *M* sodium cacodylic buffer) fixative, postfixed in osmium tetroxide, mordanted in 1% tannic acid, and stained en bloc in 0.5% uranyl acetate. The pellets were embedded in Epon, sectioned, and stained with Reynold's lead citrate and uranyl acetate. The sections were imaged on a JEOL 1220 transmission electron microscope (Jeol, Peabody, MA).

Electron Spin Resonance (ESR)

A spin trap technique was used to form long-lived free radicals that could be detected by electron spin resonance (ESR) through addition of DMPO (5,5′-dimethylpyrroline *N*-oxide). ESR measurements were collected using a flat cell assembly and Brüker EMX spectrometer (Billerica, MA). Tungstate NP were incubated at a final concentration of 1 mg/ml with 1 m*M* H_2O_2 and 100 m*M* DMPO (Sigma Chemical Co., St. Louis, MO) for 3 min as previously described (Leonard et al., 2010). Samples were run in triplicates. Signal intensity (peak height) was used to measure the relative amount of hydroxyl radicals produced and measured in mm.

For cellular ESR, tungstate NP at a final concentration of 1 mg/ml were incubated with RAW 264.7 cells at 2×10^6 cells/ml and 200 mM DMPO for 5 min at 37°C (Leonard et al., 2010). Peak heights represent relative amounts of hydroxyl radicals produced, and are measured in millimeters.

Hydrogen Peroxide Production

RAW 264.7 cells were seeded at 1×10^5 cells per well in 96-well plates and allowed to grow for 24 h until approximately 60% confluent. Assays were completed using recommended company protocol (OXIS International, Foster City, CA). Briefly, cells were exposed to tungstate NP at a final concentration of 50 μg/ml for 5 min or 1 h. Following exposure, 10 μl media was removed from the centrifuged 96 well plate and combined with 90 μl of working reagent. Following a 30-min incubation, absorbance was measured at 560 nm using a Synergy H1 Multi-Mode Microplate Reader (Bio Tek Instruments, Inc. Winooski, VT). Data are reported as percent absorbance compared to control.

Intracellular ROS Production

RAW 264.7 cells were seeded at 5×10^4 cells per well in 96-well plates and allowed to grow for 24 h until approximately 50% confluent. The assay was completed using the recommended company protocol (Cell Biolabs, Inc., San Diego, CA). Briefly, 2°,7°-dichlorodihydrofluorescin diacetate (DCFH-DA), diluted in serum-free medium, was added to cells following removal of media and 3 washes with PBS and incubated for 45 min at 37°C. Following incubation, media were removed, cells were washed with PBS, and serum-free media was added to wells with tungstate NP at a final concentration of 50 μg/ml.

Control wells were run containing only media and tungstate NP to measure potential autofluorescence, but none was detected above the fluorescence of the blank. Measurements were recorded every hour at 480 nm excitation/530 nm emission using a Synergy H1 Multi-Mode microplate reader (Bio Tek Instruments, Inc.m Winooski, VT). Data were reported in DCF fluorescence units.

Comet Assay

RAW 264.7 cells were seeded at 1×10^5 in 24-well plates and grown until 50% confluent. Cells were exposed to tungstate NP at a final concentration of 50 μg/ml for 7 h. A comet assay was completed using an alkaline system as outlined by the company (Trevigen, Gaithersburg, MD). Briefly, cells were washed with PBS, combined with preheated agarose, and placed on comet slides. Samples were lysed, treated with an unwinding solution, and electrophoresed at 21 V, 50 mA, for 50 min. Following fixation with 70% ethanol and an overnight drying stage, slides were treated with SYBR green and imaged using an Olympus AX70 microscope equipped with an Olympus DP73 digital camera (Olympus, Center Valley, PA). Experiments were completed in duplicate and at a minimum 50 comets were measured for percent DNA in comet tails. These measurements were calculated using ImageJ software to compare the corrected nuclear region fluorescence to the corrected total cell fluorescence as previously described (Collins et al., 2008; Schneider et al., 2012). These values were converted to percent DNA in the “tail.”

MTT Assay

Cells were seeded at 2.5×10^4 cells per well in 96-well plates. Following 24 h of growth, cells were exposed to tungstate NP at a final concentration of 50 μg/ml for 24, 48, or 72 h. Four hours prior to each time point, media were removed and replaced with 100 μl phenol red-free medium containing 0.5 mg/ml MTT (3-(4,5-dimethylthiazol-2-yl)-2,5-diphenyltetrazolium bromide) (Invitrogen, Carlsbad, CA). After 4 h, 50 μl media was removed and replaced with 100 μl dimethyl sulfoxide (DMSO) (Fisher Scientific, Pittsburgh, PA) to solubilize the formazan crystals, mixed, and incubated for 10 min at 37°C. Control wells were run to remove any potential background produced by the particles when incubated with the cells. No apparent absorbance background above the blank was detected. Absorbance was measured at 570 nm using a Synergy H1 Multi-Mode microplate reader (Bio Tek Instruments, Inc., Winooski, VT). Data reported as percent absorbance compared to control.

Caspase 3/7 Assay

RAW 264.7 cells were seeded at 1×10^5 cells per well in 96-well plates. Following 24 h of growth, cells were exposed to tungstate NP at a final concentration of 50 μg/ml for 24 h. The caspase 3/7 assay was completed according to company protocol (Invitrogen, Carlsbad, CA). Thirty minutes prior to the 24-h time point, 5 μ*M* caspase 3/7 reagent was added to the wells and incubated at 37°C. Fluorescence was measured at 502 nm excitation/530 nm emission using a Synergy H1 Multi-Mode microplate reader (Bio Tek Instruments, Inc., Winooski, VT). Data were reported as percent fluorescence compared to control.

Statistical Analysis

All data are represented as the mean ± standard deviation for each condition. To compare responses between groups, a one-way analysis of variance (ANOVA) and Tukey posttest were performed using GraphPad Prism 6 software (GraphPad Software, Inc., La Jolla, CA). Statistical significance is shown when $p < .05$.

RESULTS

Characteristics

Analysis by XRD indicated that all 12 tungstate NP samples were pure and contained no detectable crystalline impurities, which is in agreement with previous reports (Zhang et al., 2008a) (Supplemental Figure 1). SEM images provided length and size characteristics of the 6 different spheres and 6 different wires (Table 1 and Figure 1). All six aggregates of nanospheres were of similar sizes, with the exception of $BaWO_4$. Agglomerates of $BaWO_4$ spheres measured greater than 1 μm in diameter and 4 μm in length, while the remaining aggregated spheres were less than 400 mean nm in diameter and less than 122 mean nm in length. All 6 nanowires were of similar diameter, mean approximately 100 nm, and of similar length, mean approximately 2 μm. Although the measured diameters were found to be significantly larger than the nominal pore size of the template, expansion of the pore walls during nanowire growth is typical under U-tube conditions, particularly for polycarbonate membranes. The diameter of the nanowires is in agreement with previous reports (Koenigsmann et al., 2010, 2011, 2012).

DLS was used to assess particle size under physiological exposure conditions used in cellular exposures. Results showed the nanospheres existed in two populations, large and small with the exception of $BaWO_4$ and $Ca_7Sr_3WO_4$ nanospheres, which dispersed into a single size population (Figure 1A). In suspension, $BaWO_4$ population size was smaller than that measured under dry conditions, possibly a result of the nonspherical shape. DLS cannot accurately define the diameter of nonspherical NP, but provides a representative measurement of the wires' relative sizes and provides an indication of dispersion state (Ji et al., 2012). Results for nanowires showed that with the exception of $SrWO_4$ and $BaWO_4$, all other nanowires formed large agglomerations with diameters between 200 nm and 6000 nm. On the other hand, $SrWO_4$ and $BaWO_4$ nanowires had diameters around 1 nm, which indicates they did not form large agglomerates (Supplemental Figure 2).

Cellular Interactions With Particles Show Accumulation Over Time

To investigate potential tungstate NP cellular interactions, enhanced dark-field microscopy was used to visualize both spheres and wires with RAW 264.7 cells over a time course of 7 h. Results showed that both spheres and wires accumulated on the cell surface over the time course (Figure 2). However, the wires associated with cells more rapidly as compared with the spheres as noted at 1 h and 3 h time points. Figure 2A illustrates that after 1 h, $SrWO_4$, $Ca_3Sr_7WO_4$, $Ca_5Sr_5WO_4$, and $Ca_7Sr_3WO_4$ tungstate spheres were significantly associated with cells, relative to PBS vehicle-exposed cells. Conversely, after 1 h, all tungstate wires with the exception of $BaWO_4$ were significantly associated with cells relative to PBS vehicle control cells (Figure 2B).

Cellular Engulfment of Tungstate Nanoparticles

To study whether tungstate–cellular interactions visualized with dark-field microscopy were associated with engulfment of NP after 3 h, transmission electron microscopy (TEM) was implemented. Tungstate nanospheres were visualized within the cells, while nanowires were not. Images demonstrated that the nanospheres were engulfed and possibly confined to cytoplasmic vacuoles, rather than existing free in the cytoplasm (Figure 3). TEM images showed no engulfment of nanowires after 3 h and no changes in cellular morphology (data not shown). Based on the lack of TEM confirmation of nanowire engulfment, SEM analysis was performed to determine whether the wires attach to and penetrate the cell surface. Only $Ca_3Sr_7WO_4$, and $Ca_7Sr_3WO_4$ wires could be verified as being associated with cells (Supplemental 3A); however, examination of cells demonstrated increased cellular debris following exposure to all tungstate nanowires, suggesting the cells are likely reacting to the presence of wires. SEM displayed that nanowires either were lying on top of the cells or were protruding into the cells. Elemental analysis was completed to confirm the particles associated with the cells were actually tungstate nanowires (Supplemental 3B).

Hydroxyl Radical Production From Tungstate Nanoparticles

Based on the visualization of particle-cellular interactions occurring rapidly (within 1 h) and previous studies highlighting metal oxide-induced ROS production (Applerot et al., 2009), hydroxyl radical production was measured. To determine whether tungstate NP are capable of converting H_2O_2 to hydroxyl radicals, acellular Fenton reactions were carried out using ESR and a spin trap method. Both spheres and wires were capable of producing hydroxyl radicals in an acellular system, with $SrWO_4$ wires producing significantly more hydroxyl radicals as compared with $SrWO_4$ spheres (Figure 4A). Because hydroxyl radicals are highly reactive, their production provides a basis for cellular damage, and thus cellular ESR was also completed. Data showed that the spheres yielded no hydroxyl radical production, whereas wires, with the exception of $BaWO_4$, still produced hydroxyl radicals (Figure 4B). However, the hydroxyl radical peak height by wires decreased under cellular conditions relative to acellular production (e.g., $Ca_3Sr_7WO_4$: 57.8 ± 5 mm for H_2O_2 versus 33.2 ± 6.7 mm for cellular, mean ± SD).

Tungstate Nanoparticles on Hydrogen Peroxide Release

Based on the ESR results, it was decided to examine H_2O_2 production as another means of measuring ROS. To assess the release of H_2O_2 from cells, media were measured after 5 min and 1 h exposures with tungstate NP based on dark-field imaging showing rapid cellular association (within 1 h) and ESR demonstrating hydroxyl radical formation within 5 min. Figure 5 shows no H_2O_2 production at either time point following cellular exposure with both wires and spheres as compared with PBS controls.

Tungstate Nanowires Induce Intracellular ROS

To further explore ROS induction following tungstate NP exposure, intracellular ROS production was assessed using a cell-permeable dye, DCFH-DA, which fluoresces in the presence of ROS. Because H_2O_2 production was not measured within 1 h of tungstate NP exposure, an increased time of 7 h was used to assess intracellular ROS production. Cells

were exposed to tungstate NP (wires and spheres) and measurements were taken every hour for the 7 h exposure. Out of all six spheres, only $Ca_7Sr_3WO_4$ exposure with cells resulted in significantly increased intracellular ROS production as compared with PBS controls (PBS, 1610.5 ± 438.08, $Ca_7Sr_3WO_4$, 3148.1 ± 1332.2 at 4 h, Figure 6A). Wire-exposed cells displayed significant ROS production relative to PBS controls starting at 5 h of exposure with all 6 tungstate wires (Figure 6B).

Tungstate NP Exposure on DNA Damage

To measure potential oxidative DNA damage following NP exposure, an alkaline comet assay was used (Fairbairn et al., 1995; Hartmann and Speit, 1997). A comet assay uses an unwinding and electrophoresis process to produce comet "tails," which are formed following nuclear DNA damage. In response to intracellular ROS measurements showing significant increasing ROS production at 4 to 7 h, oxidative DNA damage was measured at 7 h. Cells exposed to tungstate NP for 7 h showed no significant DNA damage as compared with respective PBS controls (Figure 7).

Tungstate NP Exposure on Cell Viability

To measure overall cell viability following NP exposure, an MTT assay was used (Yang et al., 2009). Because no significant DNA damage was measured at 7 h of tungstate NP exposure, an increased time of 72 h of exposure was examined. At 24 h, cellular exposure with spheres showed a trend toward enhanced cell viability compared with PBS-exposed controls. In contrast, cellular exposure to wires demonstrated a trend toward decreased viability as compared with PBS controls at the same time point (Figure 8A). At 48 h, these changes in viability were no longer present with either wires-or sphere-exposed cells, with the exception of $Ca_3Sr_7WO_4$ wires, which gave a result significantly lower compared with both PBS vehicle control cells and $Ca_3Sr_7WO_4$ sphere-exposed cells (wire: 74.9 ± 8.8%, PBS control: 100 ± 6.1%, sphere: 111.6 ± 23.0%, Figure 8B). At 72 h, cellular exposure to $Ca_3Sr_7WO_4$, $Ca_5Sr_5WO_4$, and $Ca_3Sr_7WO_4$ wires induced significant reduction in viability compared with PBS vehicle control (Figure 8C). No significant differences were measured at 72 h with sphere exposures.

To determine whether these decreases in viability at 24 h of exposure were due to apoptosis, caspase 3/7 activation was measured. Measurements showed no caspase 3/7 activation by cells exposed to spheres and wires as compared with PBS controls (Figure 8D). However, significant differences in caspase activation were measured between $Ca_3Sr_7WO_4$ and $Ca_5Sr_5WO_4$ wires and spheres.

DISCUSSION

Use of metal oxide NP is increasing due to their unique chemical properties. In response to this growth in manufacturing, there is concern for potential toxicity following worker exposure during processing. Decreased size and increased surface area have been implicated in NP toxicity, especially when compared with their larger counterparts, as previously shown (Karlsson et al., 2009). Therefore, this study focused on examining how differences

in shape and size affect the toxicity of six different tungstate nanowires and six different tungstate nanospheres in an acute in vitro model.

The principal finding of the present study was that tungstate nanowires reacted with RAW 264.7 cells and resulted in ROS production and cell death after 24 h at 50 μg/ml, while nanospheres did not induce significant ROS generation or cell death at the same concentration (Figures 4, 6, and 8). These differences may be due to increased surface area, inherent anisotropic character, and size, specifically the length of wires relative to spheres (Chen et al., 2010; Nel et al., 2006; Simon-Deckers et al., 2009). Size was also an important factor in the ability of NP to associate and interact with cells; aggregates of $BaWO_4$ spheres were the largest tungstate NP tested and had the least amount of cellular association over the 7 h time course. $BaWO_4$ spheres were also not visualized by TEM within the cells. Moreover, these spheres were also less reactive, indicating that increased size and lack of cellular association and engulfment may affect toxicity. As with $BaWO_4$ spheres, $BaWO_4$ wires were also less reactive, specifically in the cellular ESR experiments. Loss of reactivity between the H_2O_2 and cellular ESR system may be a result of differences in H_2O_2 levels in an acellular, spiked reaction compared to a cellular, unspiked reaction. Further, the BaWO4 wires associated the least with cells (Figure 2), and thus 5 min of incubation may not have been sufficient time for the cells to recognize the wires and react. Further, cellular association was correlated with changes in ROS production (Zhao et al., 2011). Therefore, elevated cellular associations noted with wires compared to spheres, as visualized with enhanced dark-field microscopy (Figure 2), may be responsible for differences in ROS production.

While enhanced dark-field imaging demonstrated nanowire–cellular association, both SEM and TEM analyses could not confirm that all six wires were engulfed by or associated with cells. The intrinsic morphology of the cells rendered differentiation between wires and pseudopodia difficult. In addition, the small size of the wires may have hindered spectral analysis. While SEM could only confirm that $Ca_3Sr_7WO_4$ and $Ca_7Sr_3WO_4$ wires were associated with cells and appear to be penetrating the cells, the presence of cellular debris in images of wire-exposed cells implies that this exposure may produce some form of cellular damage (Supplemental Figure 3). Large fiber or wire-like particles, such as asbestos, were previously found to lack full engulfment by cells. Association typically results in frustrated phagocytosis, which induces ROS production (O'Neill, 2008). Given our finding that tungstate nanowires were more reactive than spheres and produced continued ROS over a 7 h time course with cells, data suggest that the fiber-like shape contributes to cellular stress. The lengths of tungstate nanowires are shorter than typical fibers that result in frustrated phagocytosis (Donaldson et al., 2010) and therefore probably do not result in true frustrated phagocytosis. However, their protrusion into the cell and continued association rather than engulfment may produce similar cellular responses, such as ROS, as measured through ESR and an intracellular ROS assay. Based on the enhanced ROS generation by wires, one expects to see a significant increase in oxidative DNA damage by wires relative to spheres (Yang et al., 2009). Unexpectedly, minimal oxidative DNA damage was noted following NP cellular exposure over a 7 h time course. This indicates that tungstate NP do not induce cellular oxidative injury regardless of ROS production by cells exposed to wires (Figure 7).

Further, a discrepancy in toxicity between wires and spheres was noted through an MTT assay. The spheres produced a trend towards increased viability at 24 h of exposure. Conversely, the cells exposed to wires displayed decreased viability at 24 h, which was significant compared to both vehicle control cells and spheres. While the MTT assay is not a direct measurement of cell viability but rather a measurement of mitochondrial function, it is possible that the measured increased viability is due to over-active mitochondria rather than elevated number of cells. By 48 and 72 h this enhanced activity or increased viability was no longer measured, possibly due to the lack of toxicity that nanospheres exert. The decrease in viability of wire exposed cells may be in response to the damaging ROS measured via both ESR and the intracellular ROS assay (Figures 4 and 6). Studies showed that ROS-induced damage resulted in cytotoxicity through mitochondrial damage and promotion of apoptosis (Jeng and Swanson, 2006). Because it was anticipated that cell death was due to apoptosis, caspase 3⁄7 levels were measured following cellular interactions with wires or spheres. Based on ROS activity following cellular interactions with wires and decreased viability, enhanced caspase 3⁄7 activation was anticipated in wire-exposed as compared with sphere-exposed cells. However, significant caspase 3⁄7 activation was not detected in either sphere or wire exposures relative to PBS controls, indicating that cell death was not in response to caspase signaling, but rather is occurring via a caspase-independent cell death pathway (Figure 8D). Surprisingly, at 48 h of exposure, neither cell death nor increased viability was observed following wire and sphere exposure with cells, suggesting that damage induced by tungstate NP exposure is short-term and manageable by cells.

While our results showed minimal toxicity, there are numerous other endpoints of NP toxicity that are commonly measured, including cytokine production and inflammation, which propagate disease. ZnO NP exposure resulted in proinflammatory cytokine production, even with minimal cytotoxic effects (Heng et al., 2011). In addition, this group showed that the shape of ZnO NP played a role in ROS production and cytokine release. Data thus predicted that perhaps ROS generation in response to nanowire exposures may promote cytokine production by cells. However, there was no measurable production of interleukin IL-6, IL-8, or tumor necrosis factor TNF-α (data not shown) following exposure, suggesting that mild ROS production produced by tungstate nanowires does not result in an inflammatory response by macrophage cells in our toxicity model.

Previous studies reported that exposure of cells with NP resulted in ROS production, cellular toxicity, inflammatory responses, and apoptosis (Hussain et al., 2012; Xia et al., 2008). While our study showed that tungstate nanowires are capable of producing mild ROS and inducing cytotoxicity within 24 h, data in general provide evidence that tungstate NP may be unreactive in cell culture, unlike other previously studied metal oxide NP (Lu et al., 2009; Park and Park, 2009; Wörle-Knirsch et al., 2006; Xia et al., 2008).

Due to dosages used in previous NP research (Kang et al., 2008), it was expected that tungstate NP might produce ROS when exposed to RAW 264.7 cells at a concentration of 50 μg⁄ml. However, macrophage cells are capable of engulfing particles to limit the level of toxicity. Therefore, RAW 264.7 cells appear to be capable of dealing with the adverse effects of tungstate NP at this concentration, such as ROS production and initial decreased viability following wire exposure. It is possible that at higher concentrations, greater adverse

effects would be observed (Hussain et al., 2005). However, higher doses no longer represent the common concentration range of 0.1–100 μg/ml used in nanotoxicology studies (Hussain et al., 2012; Jeng and Swanson, 2006). Further, longer exposures were found to result in greater toxicity, and thus increased toxicity may be seen in long-term cell culture (Huang et al., 2009). However, our study was interested in acute exposures to examine the initial cellular responses to tungstate NP.

Prior to this study, nothing was known about the toxicity of tungstate NP. Our initial findings suggest that at concentrations of 50 μg/ml, tungstate NP result in mild but repairable damage. Further, these results show that shape and size play a major role in determining reactivity, as wires produced more ROS and decreased viability at 24 h as compared with spheres, while chemical composition exerted minimal effects on differences in toxicity. These results also indicated that chemical characteristics and variability exerted little discernible effect on observed differences in cellular toxicity. The goal of this study was to assess whether tungstate NP present a hazard that could be translated into occupational exposures. Data indicate that in an acute in vitro model with RAW 264.7 cells, the toxicity of tungstate NP is minimal.

Acknowledgments

FUNDING

This project was funded by a CDC/NIOSH/Health Effects Laboratory Division Direct funding project. K. M. Dunnick acknowledges support from the National Science Foundation through the IGERT program under grant DGE-1144676. Research funding for J. M. Patete, C. Koenigsmann, and S. S. Wong was provided by the U.S. Department of Energy, Basic Energy Sciences, Materials Sciences and Engineering Division at Brookhaven National Laboratory, which is supported by the U.S. Department of Energy under contract DE-AC02-98CH10886. The authors thank Natalie Fix for her technical assistance and Michael Wolfarth for his assistance with dynamic light scattering.

References

Applerot G, Lipovsky A, Dror R, Perkas N, Nitzan Y, Lubart R, Gedanken A. Enhanced antibacterial activity of nanocrystalline zno due to increased ros-mediated cell injury. Adv Funct Mater. 2009; 19:842–852.

Chen J, Zhou H, Santulli AC, Wong SS. Evaluating cytotoxicity and cellular uptake from the presence of variously processed tio2 nanostructured morphologies. Chem Res Toxicol. 2010; 23:871–879. [PubMed: 20408587]

Chung HE, Yu J, Baek M, Lee JA, Kim MS, Kim SH, Maeng EH, Lee JK, Jeong J, Choi SJ. Toxicokinetics of zinc oxide nanoparticles in rats. J Phys Conf Ser. 2013; 429:012037.

Collins AR, Oscoz AA, Brunborg G, Gaivão I, Giovannelli L, Kruszewski M, Smith CC, Štetina R. The comet assay: Topical issues. Mutagenesis. 2008; 23:143–151. [PubMed: 18283046]

Comini E. Metal oxide nanocrystals for gas sensing. Anal Chim Acta. 2006; 568:28–40. [PubMed: 17761243]

Donaldson K, Murphy F, Duffin R, Poland C. Asbestos, carbon nanotubes and the pleural mesothelium: A review of the hypothesis regarding the role of long fibre retention in the parietal pleura, inflammation and mesothelioma. Part Fibre Toxicol. 2010; 7:5. [PubMed: 20307263]

Fairbairn DW, Olive PL, O'Neill KL. The comet assay: A comprehensive review. Mutat Res Genet Toxicol. 1995; 339:37–59.

Gibbs-Flournoy E, Bromberg P, Hofer T, Samet J, Zucker R. Darkfield-confocal microscopy detection of nanoscale particle internalization by human lung cells. Part Fibre Toxicol. 2011; 8:2. [PubMed: 21247485]

Hartmann A, Speit G. The contribution of cytotoxicity to DNA-effects in the single cell gel test (comet assay). Toxicol Lett. 1997; 90:183–188. [PubMed: 9067486]

Heng B, Zhao X, Tan E, Khamis N, Assodani A, Xiong S, Ruedl C, Ng K, Loo JC. Evaluation of the cytotoxic and inflammatory potential of differentially shaped zinc oxide nanoparticles. Arch Toxicol. 2011; 85:1517–1528. [PubMed: 21656222]

Huang S, Chueh PJ, Lin YW, Shih TS, Chuang SM. Disturbed mitotic progression and genome segregation are involved in cell transformation mediated by nano-TiO_2 long-term exposure. Toxicol Appl Pharmacol. 2009; 241:182–194. [PubMed: 19695278]

Hussain S, Al-Nsour F, Rice AB, Marshburn J, Yingling B, Ji Z, Zink JI, Walker NJ, Garantziotis S. Cerium dioxide nanoparticles induce apoptosis and autophagy in human peripheral blood monocytes. ACS Nano. 2012; 6:5820–5829. [PubMed: 22717232]

Hussain SM, Hess KL, Gearhart JM, Geiss KT, Schlager JJ. In vitro toxicity of nanoparticles in Brl 3a rat liver cells. Toxicol In Vitro. 2005; 19:975–983. [PubMed: 16125895]

Jeng HA, Swanson J. Toxicity of metal oxide nanoparticles in mammalian cells. J Toxicol Environ Health A. 2006; 41:2699–2711.

Ji Z, Wang X, Zhang H, Lin S, Meng H, Sun B, George S, Xia T, Nel AE, Zink JI. Designed synthesis of ceo2 nanorods and nanowires for studying toxicological effects of high aspect ratio nanomaterials. ACS Nano. 2012; 6:5366–5380. [PubMed: 22564147]

Kang JL, Moon C, Lee HS, Lee HW, Park EM, Kim HS, Castranova V. Comparison of the biological activity between ultrafine and fine titanium dioxide particles in RAW 264.7 cells associated with oxidative stress. J Toxicol Environ Health, A. 2008; 71:478–485. [PubMed: 18338282]

Karlsson HL, Gustafsson J, Cronholm P, Möller L. Size-dependent toxicity of metal oxide particles—A comparison between nano- and micrometer size. Toxicol Lett. 2009; 188:112–118. [PubMed: 19446243]

Koenigsmann C, Santulli AC, Sutter E, Wong SS. Ambient surfactantless synthesis, growth mechanism, and size-dependent electrocatalytic behavior of high-quality, single crystalline palladium nanowires. ACS Nano. 2011; 5:7471–7487. [PubMed: 21875051]

Koenigsmann C, Sutter E, Chiesa TA, Adzic RR, Wong SS. Highly enhanced electrocatalytic oxygen reduction performance observed in bimetallic palladium-based nanowires prepared under ambient, surfactantless conditions. Nano Lett. 2012; 12:2013–2020. [PubMed: 22452593]

Koenigsmann C, Zhou W-p, Adzic RR, Sutter E, Wong SS. Size-dependent enhancement of electrocatalytic performance in relatively defect-free, processed ultrathin platinum nanowires. Nano Lett. 2010; 10:2806–2811. [PubMed: 20608712]

Leonard S, Chen B, Stone S, Schwegler-Berry D, Kenyon A, Frazer D, Antonini J. Comparison of stainless and mild steel welding fumes in generation of reactive oxygen species. Part Fibre Toxicol. 2010; 7:32. [PubMed: 21047424]

Love, SA.; Maurer-Jones, MA.; Thompson, JW.; Lin, YS.; Haynes, CL. Assessing nanoparticle toxicity. In: Cooks, RG.; Yeung, ES., editors. Annual review of analytical chemistry. Palo Alto, CA: Annual Reviews; 2012. p. 181-205.

Lu S, Duffin R, Poland C, Daly P, Murphy F, Drost E, MacNee W, Stone V, Donaldson K. Efficacy of simple short-term in vitro assays for predicting the potential of metal oxide nanoparticles to cause pulmonary inflammation. Environ Health Perspect. 2009; 117:241–247. [PubMed: 19270794]

Monteiro-Riviere NA, Wiench K, Landsiedel R, Schulte S, Inman AO, Riviere JE. Safety evaluation of sunscreen formulations containing titanium dioxide and zinc oxide nanoparticles in UVB sunburned skin: An in vitro and in vivo study. Toxicol Sci. 2011; 123:264–280. [PubMed: 21642632]

Moon C, Park HJ, Choi YH, Park EM, Castranova V, Kang JL. Pulmonary inflammation after intraperitoneal administration of ultrafine titanium dioxide TiO_2) at rest or in lungs primed with lipopolysaccharide. J Toxicol Environ Health A. 2010; 73:396–409. [PubMed: 20155581]

Nel A, Xia T, Mädler L, Li N. Toxic potential of materials at the nanolevel. Science. 2006; 311:622–627. [PubMed: 16456071]

O'Neill LA. Immunology: How frustration leads to inflammation. Sci Signaling. 2008; 320:619.

Park EJ, Park K. Oxidative stress and pro-inflammatory responses induced by silica nanoparticles in vivo and in vitro. Toxicol Lett. 2009; 184:18–25. [PubMed: 19022359]

Porter D, Sriram K, Wolfarth M, Jefferson A, Schwegler-Berry D, Andrew ME, Castranova V. A biocompatible medium for nanoparticle dispersion. Nanotoxicology. 2008; 2:144–154.

Roberts JR, Chapman RS, Tirumala VR, Karim A, Chen BT, Schwegler-Berry D, Stefaniak AB, Leonard SS, Antonini JM. Toxicological evaluation of lung responses after intratracheal exposure to non-dispersed titanium dioxide nanorods. J Toxicol Environ Health A. 2011; 74:790–810. [PubMed: 21541881]

Rushton EK, Jiang J, Leonard SS, Eberly S, Castranova V, Biswas P, Elder A, Han X, Gelein R, Finkelstein J. Concept of assessing nanoparticle hazards considering nanoparticle dosemetric and chemical/biological response metrics. J Toxicol Environ Health, A. 2010; 73:445–461. [PubMed: 20155585]

Schneider CA, Rasband WS, Eliceiri KW. NIH Image to ImageJ: 25 Years of image analysis. Nat Methods. 2012; 9:671–675. [PubMed: 22930834]

Simon-Deckers, Al; Loo, S.; Mayne-L'hermite, M.; Herlin-Boime, N.; Menguy, N.; Reynaud, Cc; Gouget, B.; Carrieère, M. Size-, composition-and shape-dependent toxicological impact of metal oxide nanoparticles and carbon nanotubes toward bacteria. Environ Sci Technol. 2009; 43:8423–8429. [PubMed: 19924979]

Thongtem T, Kungwankunakorn S, Kuntalue B, Phuruangrat A, Thongtem S. Luminescence and absorbance of highly crystalline camoo4, srmoo4, cawo4 and srwo4 nanoparticles synthesized by co-precipitation method at room temperature. J Alloys Compound. 2010; 506:475–481.

Wörle-Knirsch JM, Kern K, Schleh C, Adelhelm C, Feldmann C, Krug HF. Nanoparticulate vanadium oxide potentiated vanadium toxicity in human lung cells. Environ Sci Technol. 2006; 41:331–336. [PubMed: 17265967]

Xia T, Kovochich M, Liong M, Mädler L, Gilbert B, Shi H, Yeh JI, Zink JI, Nel AE. Comparison of the mechanism of toxicity of zinc oxide and cerium oxide nanoparticles based on dissolution and oxidative stress properties. ACS Nano. 2008; 2:2121–2134. [PubMed: 19206459]

Yang H, Liu C, Yang D, Zhang H, Xi Z. Comparative study of cytotoxicity, oxidative stress and genotoxicity induced by four typical nanomaterials: The role of particle size, shape and composition. J Appl Toxicol. 2009; 29:69–78. [PubMed: 18756589]

Zhang F, Sfeir MY, Misewich JA, Wong SS. Room-temperature preparation, characterization, and photoluminescence measurements of solid solutions of various compositionally-defined single-crystalline alkaline-earth-metal tungstate nanorods. Chem Mater. 2008a; 20:5500–5512.

Zhang F, Yiu Y, Aronson M, Wong SS. Exploring the room-temperature synthesis and properties of multifunctional doped tungstate nanorods. J Phys Chem C. 2008b; 112:14816–14824.

Zhang H, Ji Z, Xia T, Meng H, Low-Kam C, Liu R, Pokhrel S, Lin S, Wang X, Liao YP. Use of metal oxide nanoparticle band gap to develop a predictive paradigm for oxidative stress and acute pulmonary inflammation. ACS Nano. 2012; 6:4349–4368. [PubMed: 22502734]

Zhao J, Castranova V. Toxicology of nanomaterials used in nanomedicine. J Toxicol Environ Health, B. 2011; 14:593–632.

Zhao X, Heng BC, Xiong S, Guo J, Tan TTY, Boey FYC, Ng KW, Loo JSC. In vitro assessment of cellular responses to rod-shaped hydroxyapatite nanoparticles of varying lengths and surface areas. Nanotoxicology. 2011; 5:182–194. [PubMed: 21609137]

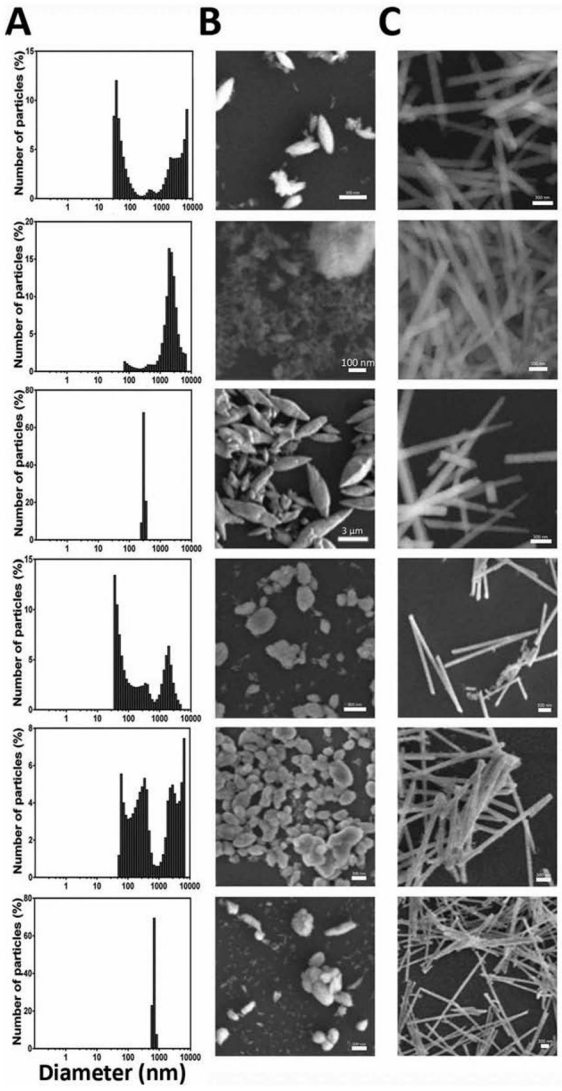

FIGURE 1.

Tungstate nanoparticle dynamic light scattering and electron microscopy images. (A) DLS was completed on tungstate nanospheres to provide diameters of the spheres in a dispersed state. (B) SEM was completed on tungstate nanospheres to provide length and size characteristics in a dry state. From top to bottom: $CaWO_4$, $SrWO_4$, $BaWO_4$, $Ca_3Sr_7WO_4$, $Ca_5Sr_5WO_4$, $Ca_7Sr_3WO_4$. (B) As in (A) except SEM was completed on analogous tungstate nanowires. All scale bars, 300 nm, except (A): second panel from top, 100 nm, third panel from top, 3 μm.

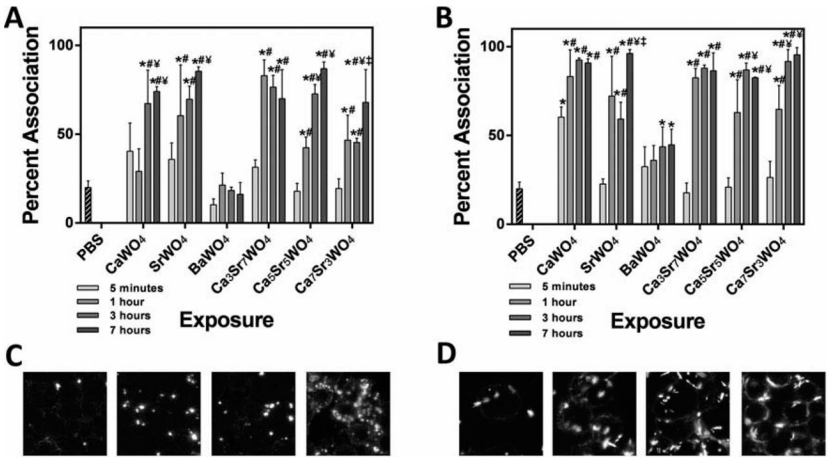

FIGURE 2.

RAW 264.7 cells associate with tungstate nanoparticles over a time course. (A) A CytoViva enhanced dark-field microscopy system provides images of high-contrast tungstate NP (bright spots) against a dark background of cells. Experiments were completed in duplicate and at a minimum, 50 cells were counted from 3 fields for each time point. Bars represent number of cells associated compared to number not associated as a percentage ± standard deviation. Asterisk indicates significant at $p < .05$ compared to PBS vehicle; #, $p < .05$ compared to 5 min; ¥, $p < .05$ compared to 1 h, ‡, $p < .05$ compared to 3 h. (B) As in (A), except cells were exposed to tungstate nanowires. (C) Representative images of cells exposed to $Ca_3Sr_7WO_4$ nanospheres over a 7 h time course. (D) As in (C), except images represent cells exposed to $CaWO_4$ nanowires over a 7 h time course. Scale bar, 10 μm.

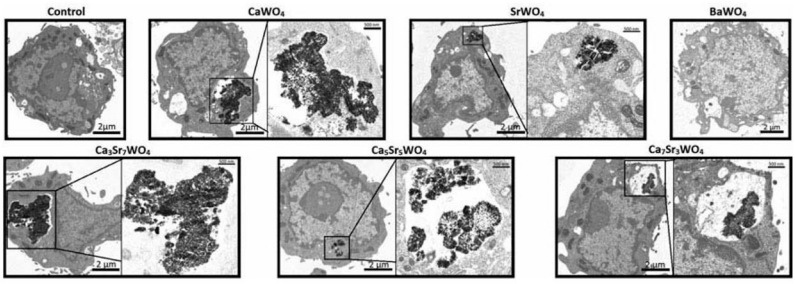

FIGURE 3.

RAW 264.7 cells engulf tungstate nanospheres. TEM analysis of RAW 264.7 cells exposed to tungstate nanospheres for 3 h.

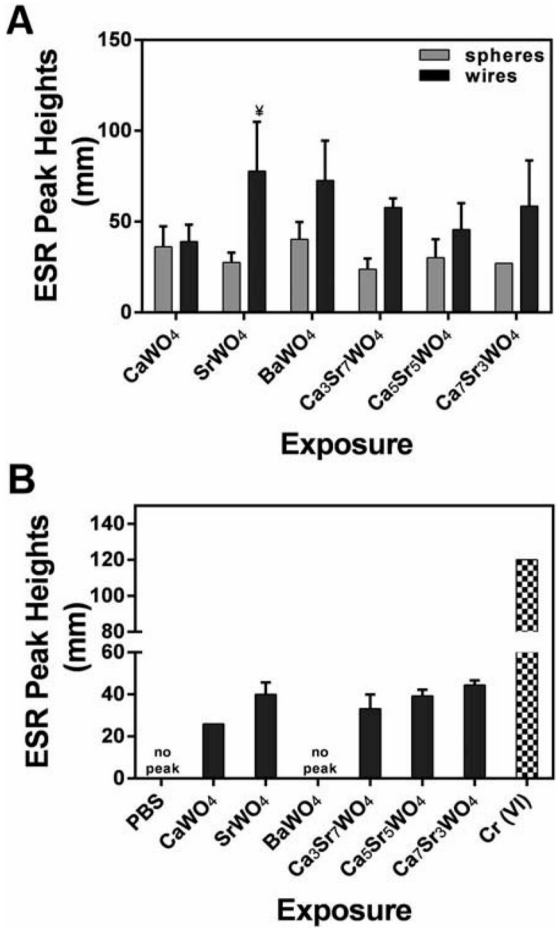

FIGURE 4.

Tungstate nanoparticles produce hydroxyl radicals. (A) Tungstate NP at 1 mg/ml were combined with 1 m*M* H_2O_2 and 100 m*M* DMPO and incubated for 3 min. ESR settings were: center field, 3385 G; scan width, 100 G; time constant, 0.25 s; modulation amplitude, 1 G; receiver gain, 2.5×10^4; frequency, 9.424 GHz; and power, 50 mW. Signal intensity was measured in millimeters. Error bars represent the mean ± standard deviation. ¥, $p < .05$ compared to spheres. (B) The same as in (A), except tungstate NP were combined with RAW 264.7 cells (2×10^6) instead of H_2O_2, and incubated for 5 min at 37°C. Bars are not shown for nanosphere exposures, as no hydroxyl radicals were produced. ESR settings were: center field, 3475 G; scan width, 100 G; time constant, 0.41 s; modulation amplitude, 1 G; receiver gain, 2.5×10^4; frequency, 9.748 GHz; and power, 126.6 mW. Error bars represent the mean ± standard deviation.

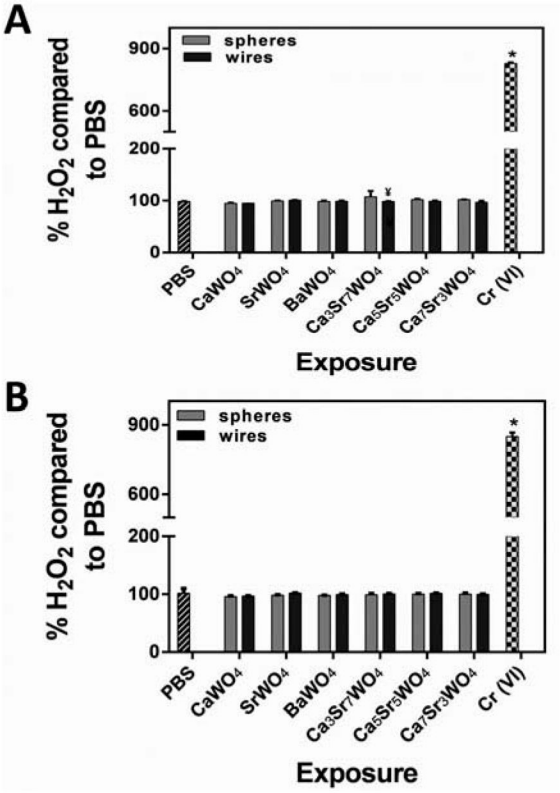

FIGURE 5.

Tungstate nanoparticles do not cause release of cellular H_2O_2. (A) RAW 264.7 cells were exposed to tungstate NP at 50 μg/ml for 5 min. Bars represent the percentage H_2O_2 production as compared with PBS control expsoed cells ± standard deviation. Asterisk indicates significant at $p < .05$ compared to PBS vehicle; ¥, $p < .05$ compared to spheres; $n = 6$. Cr(VI) at 1 m*M* was used as a positive control. (B) Same as in (A) except cells were exposed for 1 h.

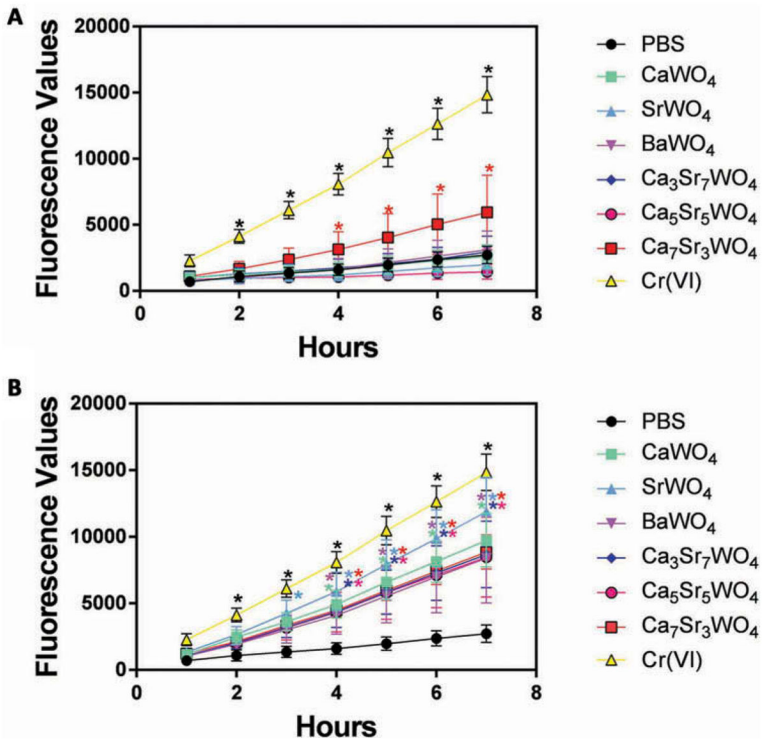

FIGURE 6.

Tungstate nanowires produce intracellular ROS. (A) RAW 264.7 cells were pretreated with DCFH-DA, then exposed to tungstate nanospheres at 50 μg/ml and incubated at 37°C for 7 h. Error bars represent mean ± standard deviation. Asterisk indicates significant at $p < .05$ compared to PBS vehicle, $n = 6$. Cr(VI) at 1 m*M* was used as a positive control. (B) Same as in (A) except cells were exposed to tungstate nanowires. Error bars represent mean ± standard deviation.

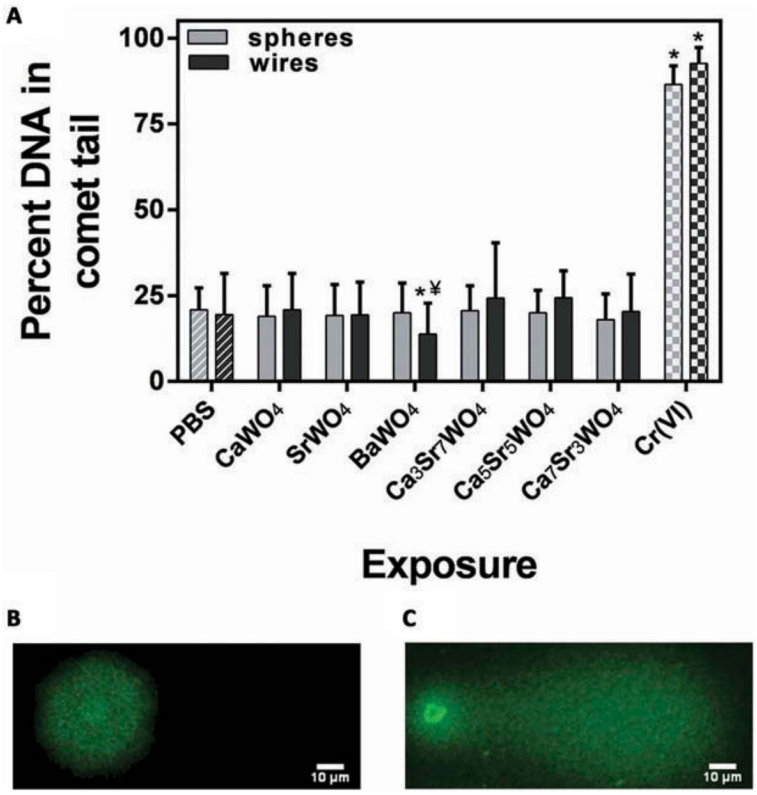

FIGURE 7.

Tungstate nanospheres do not result in oxidative DNA damage at 7 h. (A) RAW 264.7 cells were exposed to tungstate NP at 50 µg/ml for 7 h. Percent DNA in the tail was measured by comparing nuclear fluorescence with total fluorescence from images. Error bars represent the mean ± standard deviation. Asterisk indicates significant at $p < .05$ compared to PBS vehicle; ¥, $p < .05$ compared to spheres. Cr (VI) at 1 m*M* was used as a positive control. (B) Representative control cell comet. Scale bar, 5 µm. (C) Representative Cr(VI)-exposed comet.

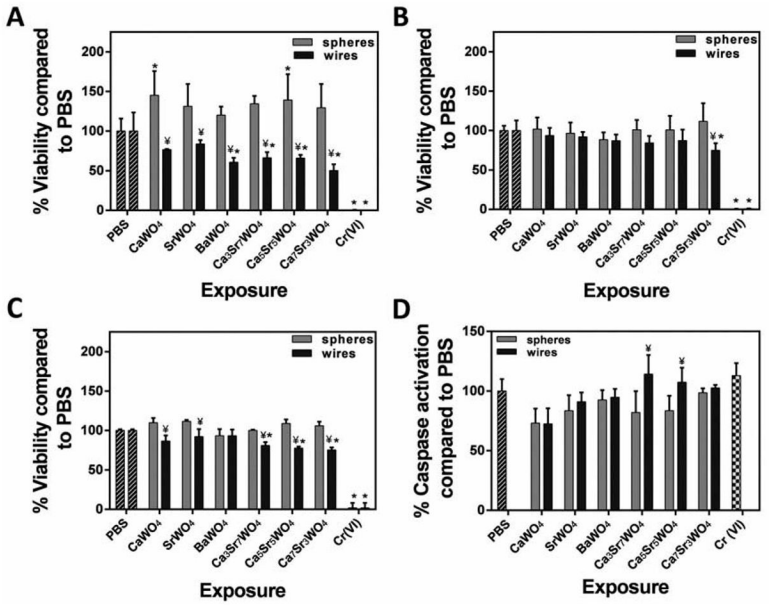

FIGURE 8.

Tungstate nanowires reduce cell viability at 24 h. (A) RAW 264.7 cells were exposed to tungstate NP at 50 μg/ml for 24 h, MTT was added 4 h prior to time point, and absorbance was measured. Error bars represent the mean ± standard deviation. Asterisk indicates significant at $p < .05$ compared to PBS vehicle; ¥, $p < .05$ compared to spheres; $n = 6$. (B) As in (A) except cells were exposed for 48 h. (C) As in (A) except cells were exposed for 72 h. (D) RAW 264.7 cells were exposed to tungstate NP at 50 μg/ml for 24 h, 5 μ*M* caspase-3/7 green detection substrate was added, and fluorescence was measured. Error bars represent the mean ± standard deviation. ¥, significant at $p < .05$ compared to spheres.

TABLE 1

Tungstate Nanoparticle Descriptive Characteristics

			LENGTH (nm)	
SAMPLE	**MORPHOLOGY**	**DIAMETER (nm)**	**LARGE**	**SMALL**
$CaWO_4$	Spheres	141 ± 59	328 ± 144	85 ± 36
$SrWO_4$	Spheres	356 ± 111	804 ± 365	32 ± 18
$BaWO_4$	Spheres	1495 ± 609	4534 ± 2223	N/A
$Ca_3Sr_7WO_4$*	Spheres	209 ± 81	278 ± 99	54 ± 17
$Ca_5Sr_5WO_4$*	Spheres	229 ± 90	320 ± 151	122 ± 59
$Ca_7Sr_3WO_4$*	Spheres	394 ± 195	394 ± 195	43 ± 18
$CaWO_4$	Nanowires	109 ± 31	2430 ± 672	N/A
$SrWO_4$	Nanowires	119 ± 26	2116 ± 1178	N/A
$BaWO_4$	Nanowires	106 ± 31	2006 ± 758	N/A
$Ca_3Sr_7WO_4$*	Nanowires	99 ± 20	2586 ± 1700	N/A
$Ca_5Sr_5WO_4$*	Nanowires	96 ± 16	1812 ± 1248	N/A
$Ca_7Sr_3WO_4$*	Nanowires	97 ± 17	2056 ± 1461	N/A

*Note. 3, 5, and 7 = 0.03, and 0.07, respectively. Data presented as mean ± standard deviation.